doi:10.22100/ijhs.v3i1.205
Original Article

IJHS 2017;3(1):19-25
ijhs.shmu.ac.ir

IJHS
International Journal of Health Studies

# Photocatalytic Degradation of 4-Nitro Phenol in Aqueous Solution by the $AgInS_2$ Nanoparticles Synthesized via Microwave Heating Technique

**Amir Hossein Cheshme Khavar [1], Moslem Jafarisani [2*]**

[1] Dept. of Basic Science, Tarbiat Modares University, Tehran, Iran.
[2] Dept. of Basic Sciences, School of Medicine, Shahroud University of Medical Sciences, Shahroud, Iran.

Received: 4 November 2016
Accepted: 8 December 2016

## Abstract

***Background:*** *With increasing demands for environmental protection, photocatalysis has attracted great attention, and AgInS2 based photocatalysis are an attractive system to study.*
***Methods:*** *In this work, AgInS2 (AIS) nanoparticles were synthesized via the microwave heating process with the power of 900 W for 5 min, which showed excellent photocatalytic activities upon the degradation of 4-nitro phenol (4-NP) under visible light irradiation.*
***Results:*** *The optimum catalyst showed the removal efficiency up to 97%, of 4-NP with the 15 mg L−1 concentration from the water after 80 min photocatalytic reaction time. The mechanism of photocatalysis was also analyzed. The product was characterized by PXRD, FE-SEM, TEM, and UV-Vis spectroscopy. A scanning electron microscope and transmission electron microscope revealed the particle morphology, with the average size of 70 nm. Powder X-ray diffraction confirmed that the resultant product is a pure orthorhombic phase of AIS nanoparticles. The band gap energy of 1.96 eV estimated by the diffuse reflectance spectroscopy (DRS), exhibited that this product can be prone for photocatalytic activity in the visible region.*
***Conclusions:*** *It is suggested that the AgInS2 nanoparticles developed in our work can provide a new platform for the design of highly efficient photocatalysts under visible light irradiation.*

**Keywords:** AIS nanoparticles; Microwave heating; 4-Nitro phenol; Photocatalytic activities.
**[*]Corresponding to:** M Jafarisani**, Email:** moslem.jafarisani@gmail.Com
**Please cite this paper as:** Cheshme Khavar AH, Jafarisani M. Photocatalytic degradation of 4-nitro phenol in aqueous solution by the $AgInS_2$ nanoparticles synthesized via microwave heating technique. Int J Health Stud 2017;3(1):19-25.

## Introduction

Nitrophenols are a category of raw materials that, despite being introduced as a toxic substance by various environmental protection agencies, is still used to produce many synthetic compounds such as pesticides, insecticides, and herbicides. Therefore, a major challenge always dealing with it is the difficult refinement of these toxic contaminants before their discharge into the environment due to their high stability and solubility in water.[1] An example of this class is 4-nitro phenol, which has its molecular structure depicted in figure 1.

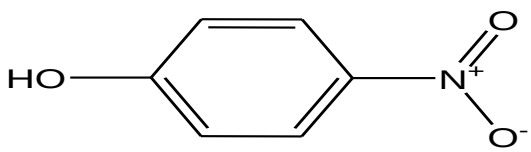


**Figure 1. The molecular structure of 4-nitro phenol**

The utilization of the photocatalysis technique in order to destroy organic pollutants in water is an interesting method that can replace traditional methods.[1-7] $TiO_2$, with band gap energy of about 3.2 eV, is introduced as a common efficient catalyst that possesses the best performance for photodegradation of organic contaminants in the ultra violet (UV) region. Whereas, UV illumination only restricts up to 5% of sunlight, the photocatalytic activity of this material is sufficiently limited.[8,9] This led us to carry out a lot of work on the other compounds that are prone to photocatalytic activity in the domain of sunlight.

In recent years, there has been significant interest in the synthesis and application of the ternary semiconductor nanomaterials instead of common photocatalysts. These materials have the general formula of XYmZn (X=Cu, Ag, Zn, Cd; Y=Ga, In; Z=S, Se, Te; m, n=integer), and this variety of low gap energy can drive the photodegradation of pollutants in visible light irradiation.[10,11] $AgInS_2$ (AIS) is one of the most promising materials of ternary chalcogenides for photovoltaic and photocatalytic applications because of its high extinction coefficient in the visible and near-infrared regions and band gap energy of about 1.86-2.04 eV matching with this area.[10-15] $AgInS_2$, as a special semiconductor, can be crystallized in two different phases containing a tetragonal, chalcopyrite type that is stable below 620˚C, and an orthorhombic phase that has a steady state at above 620˚C.[15]

Several processes are used to synthesize $AgInS_2$ nanostructures, such as solvothermal,[16,17] hydrothermal,[18] the co-evaporation method,[5] and spray pyrolysis.[19,20] Among these methods, the microwave-assisted technique has been recently employed to construct a large variety of nanomaterials. This procedure is attractive because it does not require expensive and complicated equipment.[21] Compared to conventional heating approaches, the use of a facile microwave heating approach is associated with advantages such as a short reaction time, less secondary impurities, high efficiency, and also, low-cost energy. However, microwave signals are absorbed by the atmosphere. Microwaves suffer from attenuation due to atmospheric conditions.[2,20-22] However, the application of domestic microwave ovens has had limited documentation for being employed to synthesize $AgInS_2$, while the pure phase of the product is not formed.[23,24]

In this study, the synthesis and characterization of $AgInS_2$ nanoparticles by the facile microwave heating approach is reported. Meanwhile, the photocatalytic performance of the obtained product is evaluated by photodegradation of 4-nitro

phenol (4-NP) from an aqueous medium under visible light irradiation.

## Materials and Methods

Silver nitrate ($AgNO_3$, pure), Indium (III) chloride tetrahydrate ($InCl_3.4H_2O$, pure), thioacetamide ($C_2H_5NS$, pure), sodium dodecyl sulfate ($NaCl_2H_{25}SO_4$, SDS, pure), ethylene glycol ($C_2H_6O_2$, EG, pure), and ethanol ($C_2H_5OH$, 95%) were provided as the chemicals. All of these chemicals were purchased from Merck Co. and used without further purification.

The experimental procedure was arranged in brief: 58 mg $AgNO_3$, 100 mg $InCl_3.4H_2O$, 51 mg thioacetamide and 19.6 mg SDS were separately dissolved in 10 mL ethylene glycol (EG), as a solvent, under magnetic stirring. SDS as an appropriate surfactant is used to provide the high dilution and prevent the further accumulation of particles produced in solution. After mixing the silver and indium precursors to each other, thioacetamide as a sulfur source was added to the above-prepared solution. Then, the stirring was continued for 10 min., and the prepared suspension was transferred to a domestic microwave oven. The reaction was operated by the microwave irradiation with the power of 900 Watt for 5 min. At given intervals of irradiation (1 min.) the proceeding reaction was controlled. Finally, the obtained precipitation was collected, filtered, washed several times with ethanol and distilled water, and dried at 70˚C for 4 h in a vacuum oven.

The photocatalytic behavior of the prepared AIS nanoparticles was evaluated via a probe reaction on the degradation of 4-nitro phenol in aqueous medium under visible light irradiation. A certain amount (0.02 g) of the photocatalyst for all of the experiments was separately poured into a 100 mL beaker containing 50 mL of the 4-NP solution with three different kinds of initial concentrations (15, 25, and 50 mg L−1).The adsorption-desorption equilibrium was established in the dark for 20 min. before starting the photocatalytic reaction. Then, each beaker containing a pollutant solution was magnetically stirred for a 90 min. period under light irradiation. All of the operations were performed with an initial pH adjusted to 3 with HCl. In order to adjust the pH value, three sets of the degradation reactions in different pH values (3, 6, and 9) were performed by using the 4-NP solution with a concentration of 15 mg L−1. The visible illumination was provided by a high-pressure mercury-vapor lamp (500W and λ=546.8 nm). At given intervals of irradiation (10 min.), the portions of suspension were taken away from the reaction vessels and filtered using a centrifuge. The remaining concentration of 4-nitrophenol solutions was studied by a UV-Vis spectrophotometer at the wavelengths of 315 nm.

The X-ray diffraction (XRD) patterns were recorded by a JEOL diffractometer using Cu Kα radiation (wavelength, λ=1.5418 Å). Scanning electron microscopy (SEM) images were taken on a Philips XL-30E SEM with gold coating. Transmission electron microscopy (TEM) was measured using a ZEISS EM900 microscope working at 50 kV. Fourier transform infrared (FT-IR) spectra were recorded on a Shimadzu-8400S spectrometer in the range of 400–4000 cm−1 using KBr pellets. The surface area of the product was obtained by using Brunauer-Emmett-Teller (BET) technique with Micromeritics (Gemini) in the range of relative pressures from 0.0 to 1.0. Before employing it, the sample was degassed at 200ºC for 2 h. In addition, the pore size distribution was determined from the desorption branch of the isotherm curve using the Barrett-Joyner-Halenda (BJH) model. The diffuse reflectance spectroscopy (DRS) was obtained using Shimadzu-UV-2550-8030 spectrophotometer in the range of 190–800 nm with slit width of 5.0 nm and light source with wavelength of 360.0 nm at room temperature.

## Results

The X-ray diffraction pattern of the synthesized AIS nanoparticles using the microwave approach was illustrated in figure 2. All of the diffraction peaks from the XRD pattern of figure 2 matched well with the standard Joint Committee on Powder Diffraction Standards (JCPDS) No. 25-1328 pattern of orthorhombic $AgInS_2$. Bragg's reflections for AIS nps are observed in the XRD pattern at 2θ values of 24.993°, 25.428°, 26.578°, 28.383°, 28.757°, 36.806°, 37.121°, 43.694°, 44.53°, 48.050°, 48.267°, and 52.618° matching with the 120, 200, 002, 121, 201, 122, 202, 040, 320, 123, 203, and 322 planes of the orthorhombic AIS phase. This pattern reveals the pure orthorhombic phase $AgInS_2$ without other peaks related to the impurities. Furthermore, the sharp peaks confirmed high crystallinity of the resulting product.

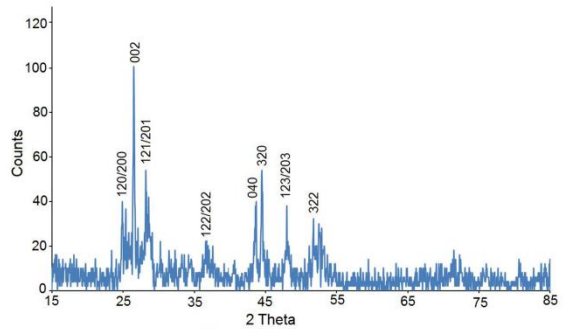


**Figure 2. The XRD pattern of AIS nanoparticles synthesized by microwave heating technique**

Figure 3 shows FT-IR spectrum of product. There are no peaks in the range of 500–4000 cm-1, which proves the formation of the pure AIS phase. All of the organic materials used in the reaction were removed by washing with ethanol and distilled water.

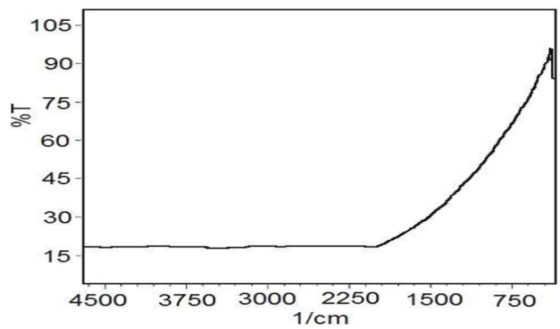


**Figure 3. FT-IR spectrum of the AIS nanoparticles**

Figure 4 indicates the SEM images of the AIS nanoparticles. These images clearly show the uniform morphology of nanoparticles, with the average particle size of 70 nm and standard deviation of 3.17, which was estimated using a microstructure measurement program and Minitab statistical software. The histogram of the particles size distribution for the as-prepared product is illustrated in figure 5. The TEM images shown in figure 6 obviously confirmed the results of the SEM image. The observed aggregation in the TEM images can be originated from the large surface area to volume ratio and small size of particles in a nanoscale.

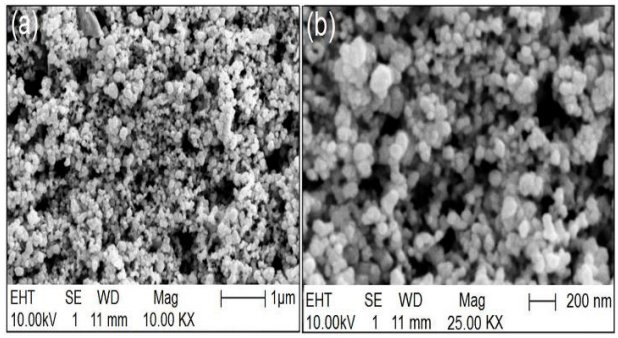


**Figure 4. SEM images of the AIS nanoparticles synthesized using thioacetamide as a sulfur source, ethylene glycol as a solvent and reaction time of 5 min**

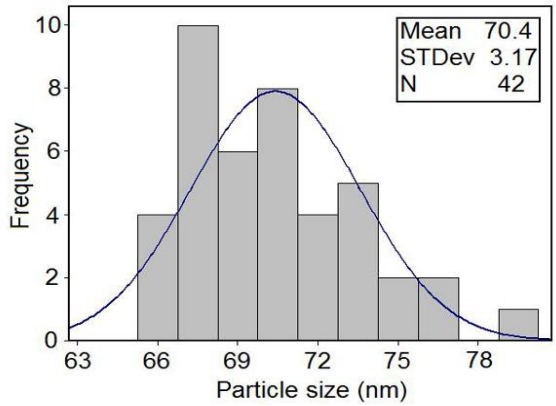


**Figure 5. The statistical graph of particle size distribution of AIS nanoparticles prepared in the optimal conditions**

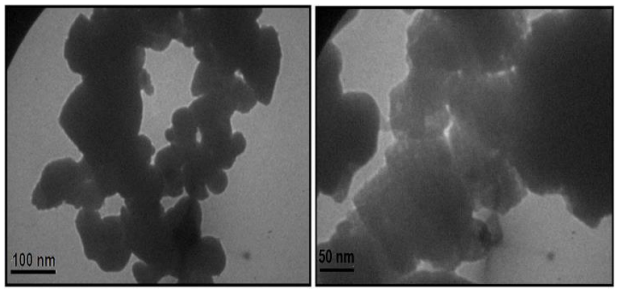


**Figure 6. TEM images of the synthesized AIS nanoparticles**

The nitrogen adsorption and desorption experiments were performed for determining the surface area of these nanoparticles. A distinct hysteresis loop recorded at the range of 0<P/P0<1 indicated the category of type V (figure 6). The Brunauer-Emmett-Teller (BET) surface area about 5.9 m2g−1 was calculated for the AIS nanoparticles synthesized in this work. The Barrett-Joyner-Halenda (BJH) model, using the desorption branch of the nitrogen isotherm, was used to evaluate the pore size distribution of the AIS nanoparticles, which is centered at 1.64 nm (inserted in the inset of figure 7). This value is higher than the reported values in various literatures for this compound,[2] and it reveals the presence of active sites on the surface of this product. So, this product can be applied as a nearly good photocatalyst to remove organic pollutants from aqueous solutions.

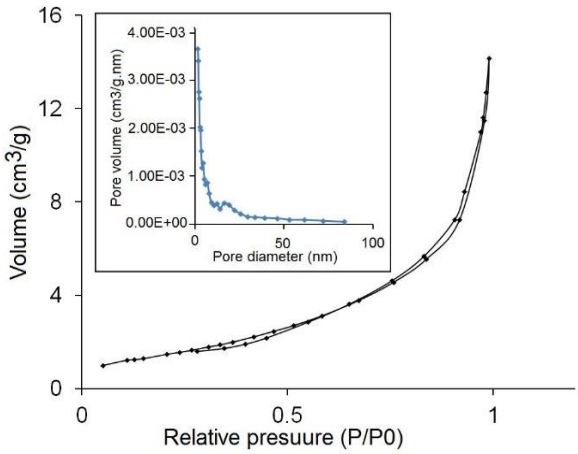


**Figure 7. Nitrogen adsorption (♦) and desorption (▲) isotherms for timber-like nanostructure. The inset shows BJH plot of this product**

The optical characteristic of the synthesized AIS nanoparticles was investigated via estimating the direct band gap energy. The band gap energy of 1.96 eV for this compound was figured out from the extrapolating of (αhν)2 vs. hν plot (figure 8) based on the UV-Vis absorption spectrum (In the inset of this figure). In fact, this parameter is calculated by the following Tauc relation:[25]

$$(\alpha h\nu)^n = B(h\nu - E_g), \quad (1)$$

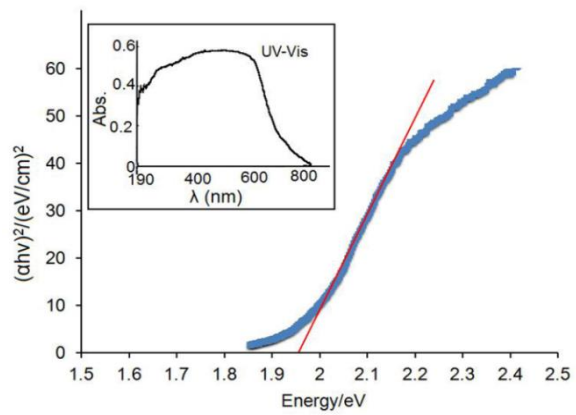


**Figure 8. The plot of $(\alpha h\nu)^2$ vs. hν (eV) for determining the direct band gap energy of the AIS nanoparticles with UV-Vis spectrum in the inset**

Where B is a constant value, α is the absorption coefficient, hν is the photon energy, and $E_g$ is the band gap energy. The value of n is assigned to the transition, which is 2 and 1/2 for direct and indirect band gap energies, respectively. In this equation, the absorption coefficient (α) is estimated by the equation (2) as follows:

$$\alpha = \frac{-1}{t} 1nT \quad (2)$$

Where T is the transmittance value and t is the substance thickness used for recording the diffuse reflectance spectrum. This nanomaterial with the band gap energy of 1.96 eV can be liable for the photocatalytic activity in the visible light area.

The photocatalytic behavior of the as-prepared AIS nanoparticles was evaluated by the degradation of 4-nitro phenol (4-NP) as a contamination model from the aqueous solution under visible light irradiation. The removal efficiency is concluded from Eq. 1:

$$\text{Removal efficiency} = \frac{C_0 - C_t}{C_0} \times 100\%, \quad (3)$$

Where $C_0$ is the initial concentration of the pollutant, and $C_t$ is the concentration of pollutant in the various irradiation times. All $C_0$ and $C_t$ values were determined by the maximum absorption at the wavelength of 315 nm. UV-Vis spectroscopy was used to monitor the changes of the photocatalytic degradation of 4-NP under visible light illumination.

Figure 9 illustrates the dependence of 4-NP degradation to the presence of catalyst and light irradiation. No degradation of 4-NP was observed in the absence of a photocatalyst under visible light irradiation. The partial value of the 4-NP concentration (about 9%) was reduced after running the photocatalytic reaction in the dark, which can be referred to the partial adsorption of organic molecules on the surface of photocatalyst particles. During the photocatalytic activity, this value of adsorption is eliminated. It is clearly observed that the degradation percentage of 4-NP raises to 97% in the presence of AIS nanoparticles under visible light illumination.

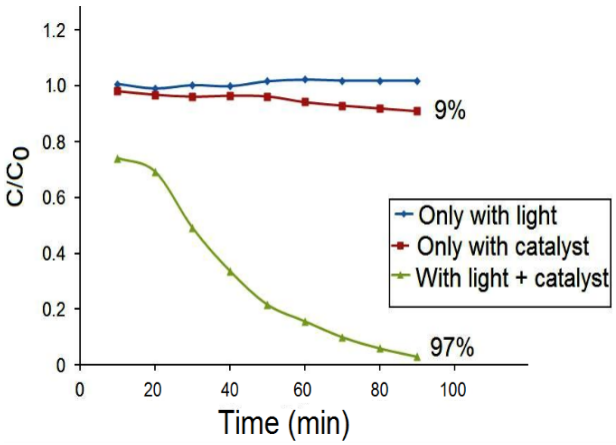


**Figure 9. Dependence of degradation of 4-NP to the presence of light and catalyst**

The effect of solution pH on the degradation of 4-NP was investigated via adjusting the solution pH in three values of 3, 6, and 9 by using 0.01 mol L−1 HCl and NaOH, respectively. Each of these runs were performed in the aqueous solutions of 4-NP with 15 mg L−1 concentration (50 mL) containing 0.02 g of the AIS photocatalyst. The highest removal efficiency of 4-NP (%93) was observed in a pH of 3, and as a result of this screening, the initial pH was adjusted to 3 for each run (figure 10).

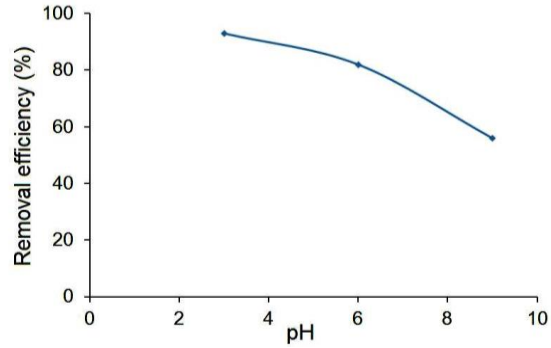


**Figure 10. The effect of pH on the degradation percentage**

To determine the optimum amount of photocatalyst, a series reaction was carried out at the solutions containing various amounts of AIS nanoparticles. The dosage range was selected from 0.005 to 0.03 g in a 50 mL solution of 4-NP (25 mg L−1) and an irradiation time of 60 min.

The results indicated that the increasing amount of photocatalyst from 0.005 to 0.02 g significantly enhanced the degradation of the pollutant. However, the further increasing led to an insignificant change in decomposition (shown in figutr 11). Therefore, the optimum amount of photocatalyst for removing 4-NP from an aqueous solution was fixed at 0.02 g.

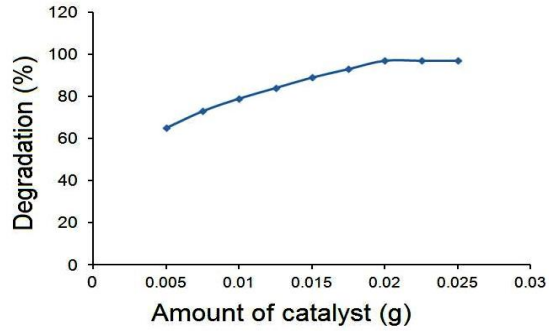


**Figure 11. The effect of photocatalyst amount on the removal efficiency**

The initial concentration effect of 4-NP for a photocatalytic reaction on the AIS nanoparticles was examined through operating three experiments with different concentrations of 15, 25, and 50 mg L−1. The results are exhibited in figure 12. It was highly considered that the value of this parameter in a low concentration of 15 mg L−1 (97%) is nearly similar to the percentage of a 25 mg L−1 concentration (93%), and the related plots have a minor difference. Whereas, increasing the 4-NP concentration from 25 to 50 mgL−1 leads to reduce the active sites over the catalyst surface and subsequently, decreases the amount of hydroxyl radicals (OH•) in the media. This decreased the degradation percentage of 4-NP to 79%.

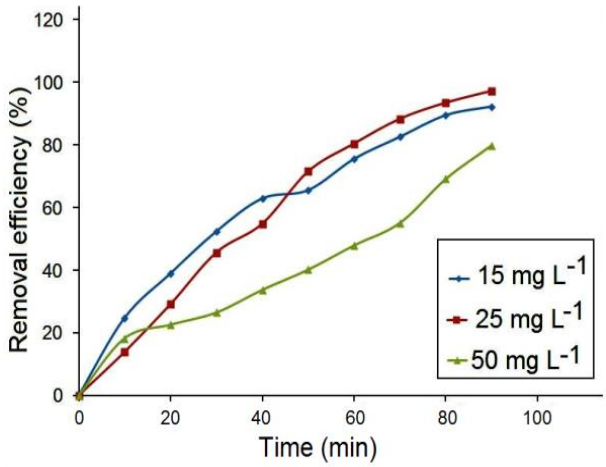


**Figure 12. Dependence of removal efficiency to initial concentration of 4-NP solution in various irradiation times**

The kinetic model of photodegradation of 4-NP was described by the following relation:

$$\mathrm{Ln}\left(\frac{C_t}{C_0}\right) = -\mathrm{Kt}, \qquad (4)$$

Where $C_0$ is the initial concentration (mg L−1) and $C_t$ is the concentration in the various reaction times, t is the slope, and k is the apparent rate constant.

By plotting $\ln(C_t/C_0)$ versus time (shown in figure 13), a linear relationship was observed for each of the three experiments with different concentrations. This represents that the photocatalytic activity of the AIS nanoparticles for removing 4-NP from aqueous mediums follows pseudo-first-order kinetics. It should be noted that the highest value of rate constants belongs to the sample with the 25 mg L−1 concentration of 4-NP. This data is in close accordance to figure. 12.

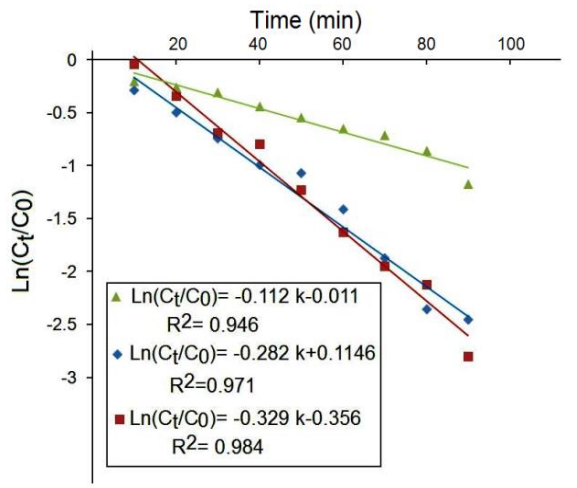


**Figure 13. The kinetics models of three samples running in three different concentrations of 15, 25, 50 mg $L^{-1}$**

Generally, in a photocatalytic process, the excitation of electrons from valence band (VB) to conduction band (CB), and the generation of electron–hole pairs, takes place on the surface of the photocatalyst by exposing it to light irradiation. The excited electrons in CB and hole (h+) in VB are captured by oxygen molecules and $OH^-$ or H2O species dissolved in the suspension, respectively. The transfer of electrons to oxygen molecules generates the superoxide anion, and also, the presence of h+ on the surface of the semiconductor leads to the production of hydroxyl radical (OH•). These species depredate the organic pollutant adsorbed on the catalyst surface. In fact, the attack of produced radicals to the aromatic ring of the 4-NP molecule leads to denitration and substitution by hydroxyl radicals. This process leads to the oxidation and decomposition of the aromatic ring and subsequently transforms to $H_2O$ and $CO_2$ species.[26] Figure 14 presents the probable mechanism of the photodegradation of 4-NP on the AIS surface.

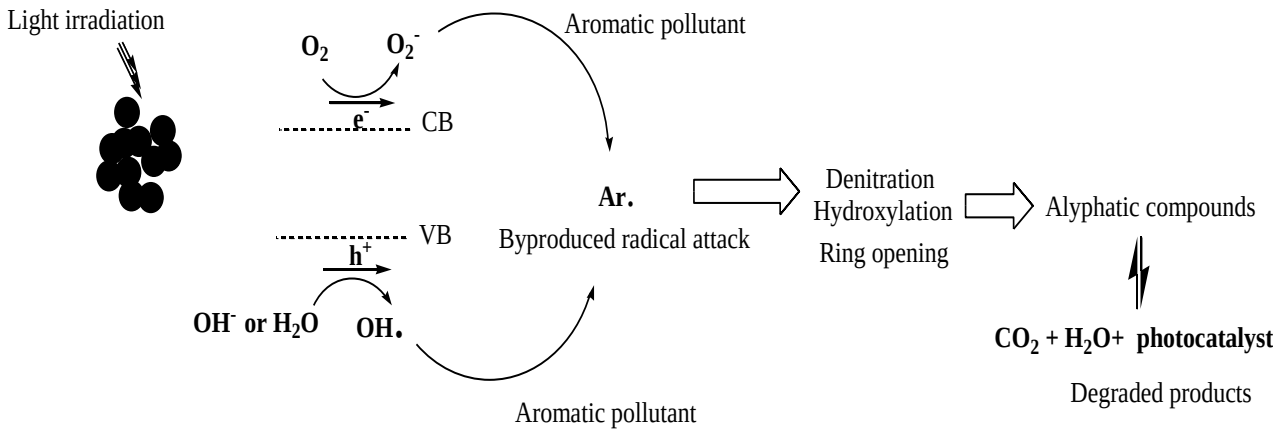


**Figure 14. The probable mechanism of photocatalytic degradation of 4-NP on the surface of AIS nanoparticles under visible light irradiation**

## Discussion

The AIS nanoparticles were employed for the photocatalytic degradation of 4-NP from an aqueous solution under visible light illumination. These nanoparticles were constructed by an efficient microwave heating technique. The pure orthorhombic phase for the resulting product was clearly shown by the XRD pattern. SEM and TEM images exhibited the particle morphology with the average size of 70 nm for this specimen. The band gap energy of the prepared compound (1.96 eV) was calculated based on UV-Vis spectrum, which completely fit to the sunlight region. The effective parameters of the photocatalytic performance on the surface of nanoparticles were studied. The highest removal efficiency (97%) was obtained in a 50 mL aqueous solution of 4-NP with the 25 mg L−1 concentration containing 0.02 g of the photocatalyst nanoparticles. As a result of evaluating the effect of pH values on the degradation percentage, the solution pH was fixed to 3. These experiments show that this compound can be nominated as a good photocatalyst in the visible light area, and due to its advantages, it can be an excellent replacement for other catalysts.

Zhang et al. [19] demonstrated the complete removal of methyl orange from an aqueous solution for $AgInS_2$ nanoparticles synthesized by a hydrothermal method. This result was achieved for 80 mg adsorbent, 5 ppm dye concentration and 9 h reaction time 2. The higher photo degradation efficiency of the present study can be related to the morphological properties and synthesis technique. Using the microwave heating method, the prepared nanoparticles were fully crystalline, spherical, and excellently monodispersed. A great importance is attached to the investigation of the aggregation state, size, shape, and morphology of the nanomaterials. The structure, morphology, and size distribution of the nanostructures is influenced by the corresponding preparation conditions. Numerous studies have already proved that the shape and the size of the nanoparticles determines the photocatalytic efficiency of the nanomaterials. The spherically monodispersed morphology plays a key role in low-light scattering at the surfaces and high packing densities. Moreover, the photocatalytic particles, which are smaller in size, involve further active surface sites and reveal more efficiency in surface charge carrier transfer. As a result, the number of surface active sites increases, and thus the 4-NP degradation rate considerably enhances. It is widely known that the catalytic process is mostly associated with the adsorption and molecular desorption on the catalytic surface. Furthermore, the results revealed that the surface area of synthesized AIS nanoparticles is larger than previous reports, and the larger surface area leads to more active sites over the catalyst surface and better photodegradation performance.

## Acknowledgement

The financial support of this study, by Tarbiat Modares University and Iranian Nanotechnology Initiative, is gratefully acknowledged

## Conflict of Interest

The authors declared that they have no conflict of interest.

## References

1. Marais E, Klein R, Antunes E, Nyokong T. Photocatalysis of 4-nitrophenol using zinc phthalocyanine complexes. Journal of Molecular Catalysis A: Chemical 2007;261:36-42. doi:10.1016/j.molcata.2006.07.055

2. Zhang W, Li D, Chen Z, Sun M, Li W, Lin Q, Fu X. Microwave hydrothermal synthesis of AgInS2 with visible light photocatalytic activity, Materials Research Bulletin 2011;46:975-82. doi:10.1016/j.materresbull.2011.03.026

3. Mele G, Del Sole R, Vasapollo G, García-López E, Palmisano L, Schiavello M. Photocatalytic degradation of 4-nitrophenol in aqueous suspension by using polycrystalline TiO2 impregnated with functionalized Cu(II) -porphyrin or Cu(II)-phthalocyanine. Journal of Catalysis 2003;217:334-342. doi:10.1016/S0021-9517(03)00040-X

4. Mele G, Ciccarella G, Vasapollo G, García-López E, Palmisano L, Schiavello M. Photocatalytic degradation of 4-nitrophenol in aqueous suspension by using polycrystalline TiO2 samples impregnated with Cu(II)-phthalocyanine. Applied Catalysis B: Environmental 2002;38:309-19. doi:10.1016/S0926-3373(02)00060-7

5. Wang C, Li J, Mele G, Yang GM, Zhang FX, Palmisano L, Vasapollo G. Efficient degradation of 4-nitrophenol by using functionalized porphyrin-TiO2 photocatalysts under visible irradiation. Applied Catalysis B: Environmental 2007;76:218-26. doi:10.1016/j.apcatb.2007.05.028

6. Moro P, Donzello MP, Ercolani C, Monacelli F, Moretti G. Tetrakis-2,3-[5,6-di-(2-pyridyl)-pyrazino]porphyrazine, and its Cu(II) complex as sensitizers in the TiO2-based photo-degradation of 4-nitrophenol. Journal of Photochemistry and Photobiology A: Chemistry 2011;220:77-83. doi:10.1016/j.jphotochem.2011.03.023

7. Huang H, Gu X, Zhou J, Ji K, Liu H, Feng Y. Photocatalytic degradation of Rhodamine B on TiO2 nanoparticles modified with porphyrin and iron-porphyrin. Catalysis Communications 2009;11:58-61. doi:10.1016/j.catcom.2009.08.012

8. Chen Y, Dionysiou DD. Effect of calcination temperature on the photocatalytic activity and adhesion of TiO2 films prepared by the P-25 powder-modified sol-gel method. Journal of Molecular Catalysis A: Chemical 2006;244:73-82. doi:10.1016/j.molcata.2005.08.056

9. Ge L, Xu M, Sun M, Fang H. Fabrication and characterization of nano TiO2 thin films at low temperature. Materials Research Bulletin 2006;41:1596-603. doi:10.1016/j.materresbull.2006.02.033

10. Mao B, Chuang CH, Wang J, Burda C. Synthesis and photophysical properties of ternary I–III–VI $Agins_2$ nanocrystals: intrinsic versus surface states. The Journal of Physical Chemistry C 2011;115:8945-54. doi:10.1021/jp2011183

11. Calixto-Rodriguez M, Martínez H, Calixto ME, Peña Y, Martínez-Escobar D, Tiburcio-Silver A, Sanchez-Juarez A. Optical and electrical characterization of AgInS2 thin films deposited by spray pyrolysis. Materials Science and Engineering: B 2010;174:253-6. doi:10.1016/j.mseb.2010.03.038

12. Tian L, Vittal JJ. Synthesis and characterization of ternary AgInS2 nanocrystals by dual- and multiple-source methods. New Journal of Chemistry 2007;31:2083-7. doi:10.1039/B707960E

13. Aguilera A, Hernández A, Trujillo G, López O, Puente C. Photoluminescence studies of chalcopyrite and orthorhombic $AgInS_2$ thin films deposited by spray pyrolysis technique. Thin Solid Films 2007;515:6272-5. doi:10.1016/j.tsf.2006.12.106

14. Wada T, Kinoshita H, Kawata S. Preparation of chalcopyrite-type CuInSe2 by non-heating process. Thin Solid Films 2003;431-432:11-5. doi:10.1016/S0040-6090(03)00231-1

15. Yoshino K, Komaki H, Kakeno T, Akaki Y, Ikari T. Growth and characterization of p-type $AgInS_2$ crystals. Journal of Physics and Chemistry of Solids 2003;64:1839-42. doi:10.1016/S0022-3697(03)00097-0

16. Cui Y, Ren J, Chen G, Qian Y, Xie Y. A simple route to synthesize MInS 2 (M = Cu, Ag) nanorods from single-molecule precursors. Chemistry Letters 2001;30:236-7. doi:10.1246/cl.2001.236

17. Hu J, Lu Q, Tang K, Qian Y, Zhou G, Liu X. Solvothermal reaction route to nanocrystalline semiconductors AgMS2 (M=Ga, In). Chemical Communications 1999;1093-4. doi:10.1039/A902218J

18. Hu JQ, Deng B, Tang KB, Wang CR, Qian YT. Preparation and phase control of nanocrystalline silver indium sulfides via a hydrothermal route. Journal of Materials Research 2001;16:3411-5. doi:10.1557/JMR.2001.0469

19. Calixto-Rodriguez M, Martínez H, Calixto ME, Pena Y, Martínez-Escobar D, Tiburcio-Silver A, et al. Optical and electrical characterization of AgInS2 thin films deposited by spray pyrolysis. Materials Science and Engineering B 2010;174:253-6.

20. Ge S, Shui Z, Zheng Z, Zhang L. A general microwave-assisted nonaqueous approach to nanocrystalline ternary metal chalcogenide and the photoluminescence study of CoIn2S4. Optical Materials 2011;33:1174-8. doi:10.1016/j.optmat.2011.02.004

21. Birkel A, Darago LE, Morrison A, Lory L, George NC, Mikhailovsky AA, Birkel CS, Seshadri R. Microwave assisted preparation of $Eu^{2+}$-doped Åkermanite $Ca_2MgSi_2O_7$. Solid State Sciences 2012;14:739-45. doi:10.1016/j.solidstatesciences.2012.03.014

22. Lekse JW, Pischera AM, Aitken JA. Understanding solid-state microwave synthesis using the diamond-like semiconductor, AgInSe2, as a case study. Materials Research Bulletin 2007;42:395-403. doi:10.1016/j.materresbull.2006.09.025

23. Landry CC, Lockwood J, Barron AR. Synthesis of chalcopyrite semiconductors and their solid solutions by microwave irradiation. Chemistry of Materials 1995;7:699-706. doi:10.1021/cm00052a015

24. Köseoğlu Y, Alan F, Tan M, Yilgin R, Öztürk M. Low temperature hydrothermal synthesis and characterization of Mn doped cobalt ferrite nanoparticles. Ceramics International 2012;38:3625-34. doi:10.1016/j.ceramint.2012.01.001

25. Manickathai K, Viswanathan SK, Alagar M. Synthesis and characterization of CdO and CdS nanoparticles, Indian Journal of Pure & Applied Physics 2008;46:561-4.

26. Wei L, Zhu H, Mao X, Gan F. Electrochemical oxidation process combined with UV photolysis for the mineralization of nitrophenol in saline wastewater. Separation and Purification Technology 2011;77:18-25. doi:10.1016/j.seppur.2010.11.007